# Oxide/polymer nanocomposites as new luminescent materials

D. Vollath, D.V. Szabó and S. Schlabach
*Forschungszentrum Karlsruhe, Institut fuer Materialforschung III, P.O. Box 3640, D-76021 Karlsruhe, Germany (E-mail: dieter.vollath@nanoconsulting.de)*

*Key words:* oxide/polymer nanocomposite, interface, quantum confinement, blue shift luminescence

**Abstract**

It is demonstrated that nanocomposites, consisting of an electrically insulating oxide core and PMMA coating exhibit strong luminescence. This luminescence is connected to the interface, where PMMA is bond via a carboxylate bonding to the surface. In this case, luminescence is originated at the carbonyl group of the coating polymer. With decreasing particle size, this emission shows a blue shift, following a law inversely the ones found for quantum confinement systems. For semi-conducting oxides, such as ZnO, this interface related emission is found additionally to quantum confinement phenomena.

## Introduction

Luminescence is one of the most important properties of nanoparticles. Applications are found primarily in medical, biological, or pharmaceutical areas. In general, luminescence is a property of aromatic organic molecules or single isolated semi-conducting nanoparticles. With respect to nanoparticles, quantum dots based on sulphides, selenides, or tellurides of zinc and cadmium show the best luminescence efficiency (Tian et al., 1996; Porteanu et al., 2001). These materials are as well toxic as carcinogenic and show limited thermodynamic stability against oxidation. These severe disadvantages make application difficult. Therefore, search for non-toxic luminescent oxide nanoparticles based on zinc oxide (Chen et al., 1997; Monticone et al., 1998; Guo et al., 2000) or other rare earth doped oxides is under way (Wang et al., 2000). Looking at potential applications, there is a strong need for non-toxic oxide luminescent nanocomposites that are stable in water.

Luminescence of oxide nanoparticles is subject of rapid aging caused by formation of hydroxides at the surface of oxide nanoparticles, quenching luminescence. Coating of the surface of the particles with a polymer protects the surface of the oxide nanoparticles against the ambient air, even against water avoids, or at least reduces this problem (Vollath, 2001; Vollath et al., 2002). Additionally, polymer-coated oxide nanoparticles can be suspended in water, most important in biological applications. In this paper, it is demonstrated that polymer-coated oxide nanoparticles have the potential to replace toxic luminescent materials.

## Experimental results

### *Polymer coating*

The Karlsruhe Microwave Plasma Process is capable to synthesize ceramic nanoparticles coated with a ceramic (Vollath, 1994; Vollath & Szabó, 1994) or a polymer (Vollath et al., 1998) layer. This process coats each single particle individually. This is a logical consequence of the physics of particle formation, as after synthesis, the particles are carrying electric charges of equal sign. Therefore, the particles repel each other avoiding agglomeration. Coating of the particles is performed in a second step of a cascaded process of synthesis. This is a statistical, gas kinetic process that is random and not directed, therefore, leading to coatings

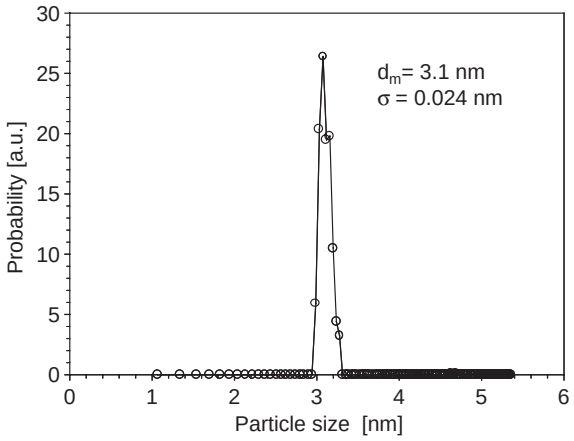


*Figure 1*. Narrow particle size distribution in nano-$ZrO_2$ particles produced by the Karlsruhe Microwave Plasma Process. The particle size distribution was measured by particle Mass Spectroscopy (Roth, 2000).

of uniform thickness. Particle size can be adjusted in the range between 3 and 10 nm; in special cases, sizes down to 2 nm are possible. It is important to realize that the size distribution gets narrower with decreasing particle size. A typical example for a particle size distribution determined by particle mass spectrometry is given in Figure 1 (Roth, 2000). The thickness of the coating is in the range from 0.5 to 2 nm for ceramic and 1–5 nm for polymer coatings (Vollath et al., 1998; 1999).

The ceramic particles are formed from the vapour of a precursor in a microwave plasma zone. Typical precursors for the ceramic kernels are water-free chlorides, carbonyls, or metal organic compounds. The selection depends on the intended properties of the final product. For the polymer coating, methacrylic acid (MAA, $H_2C{=}C(CH_3)CO{-}OH$), methylmethacrylate (MMA, $H_2C{=}C(CH_3)CO{-}O{-}CH_3$), and hydroxypropylmethacrylate (HPMA, $H_2C{=}C(CH_3)CO{-}O{-}(C_3H_6){-}OH$) monomers were the precursors. At the surface of the particles, under the influence of temperature and UV-radiation from the plasma the monomers are polymerising. Evaporated $C_{20}F_{42}$ was the starting material to coat kernels with a fluorinated polymer.

Using polymer-coated nanoparticles as functional materials; two points are of great importance: (i) the ceramic cores must not touch each other and (ii) the ceramic cores must be covered completely. Both requirements are fulfilled with the material produced according to the Karlsruhe Microwave Plasma Process. A further important point is the characterization of the polymer. Independent of the precursor, MAA or

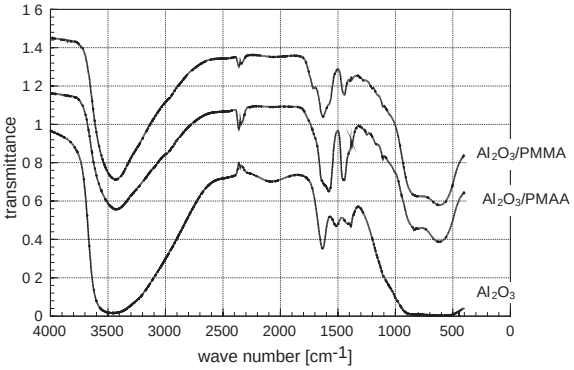


*Figure 2*. FT–IR spectra (KBr) of uncoated $Al_2O_3$ nanoparticles and of $Al_2O_3$ nanoparticles with polymer coatings derived from MAA and MMA.

MMA, only 5–10% of the polymer coating on the kernels is soluble in tetrahydrofurane (THF). The dissolved parts of the polymer are oligomers consisting of 2–5 monomer molecules (Vollath et al., 1999; Lamparth et al., 2002). A more detailed characterization was made by infrared absorption spectroscopy. Figure 2 displays the FT–IR spectra obtained from alumina kernels coated with polymers derived from MAA or MMA, respectively, in comparison to uncoated $Al_2O_3$ particles. (Lamparth et al., 2002) The spectra of polymer-coated particles exhibit almost identical spectral features with different intensity for both systems. In both spectra, bands or shoulders are observed at 1628, 1587, and 1444 $cm^{-1}$. The signals found at 1587 and 1444 $cm^{-1}$ are attributed to asymmetric and symmetric stretching vibrations of $COO^-$ usually found in compounds of this type (Socrates, 1994). The C=O vibration of the ester carbonyl group for bulk PMMA usually found at a wavenumber of 1739 $cm^{-1}$ (Konstadinidis et al., 1992) is observed very weakly in the PMMA coated material. The vibrations at 1628 $cm^{-1}$ are assigned to molecular water adsorbed (1630 $cm^{-1}$, Faguy et al., 1992; 1628 $cm^{-1}$, Pandya et al., 1994) on the surface of the ceramic particle. The most important difference between the spectrum of PMAA and PMMA coated particles is an additional shoulder at 1700 $cm^{-1}$ due to the ester carbonyl vibration visible in the $Al_2O_3$/PMMA spectrum. This is a residue of the MMA precursor. The comparison with the signals obtained from the pure alumina leads to the conclusion that the other features are due to metal oxide vibrations of the ceramic core and artefacts stemming from specimen preparation. Based on these results, one may assume that the

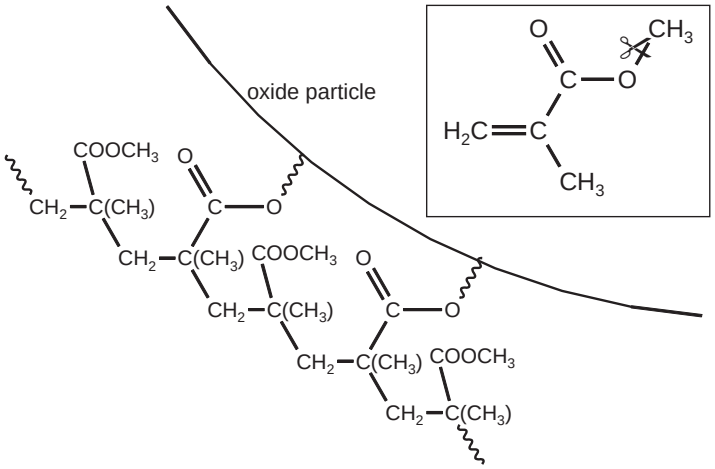


*Figure 3.* Structure formula of MMA and a model of the connection of the m-PMMA polymer to the particle.

PMMA directly touching the oxide surface is bound with an ester like linkage (Weng et al., 2003; Meyer et al., 1994) to the surface. Therefore, in the following text, the polymer at the surface is denominated as modified PMMA (m-PMMA). Based on these results, nanocomposite particles consisting of an oxide core bond to a m-PMMA may be described as one molecule, R–(C=O)–O– (oxide particle). The structure formula of MMA and a model of the connection of the polymer to the particle are given in Figure 3.

*Luminescence*

A Czerny–Turner monochromator connected to a photomultiplier tube was applied to analyse the luminescence spectra. For excitation, a HeCd laser (325 nm) or a xenon-lamp in connection with a monochromator was used. Interestingly, most of the oxides exhibit luminescence when coated with a polymer. For demonstration, Figure 4 displays the luminescence of different oxide nanoparticles coated with m-PMMA as powder. It is obvious that different oxides give rise to different luminescence intensities of the powder. As can be seen clearly, $HfO_2$ nanoparticles exhibit the highest and $WO_x$ nanoparticles the lowest luminescence intensity. Except for the tungsten oxide, the particle size of the ceramic cores was in the range of 5 nm. $\gamma$-$Fe_2O_3$/m-PMMA nanocomposites, not drawn in this figure, show no luminescence at all. It is remarkable that in contrast to the intensity, the position of the luminescence intensity maximum depends only weakly on the oxide core. Some of these spectra are influenced by concentration quenching; the most striking example for

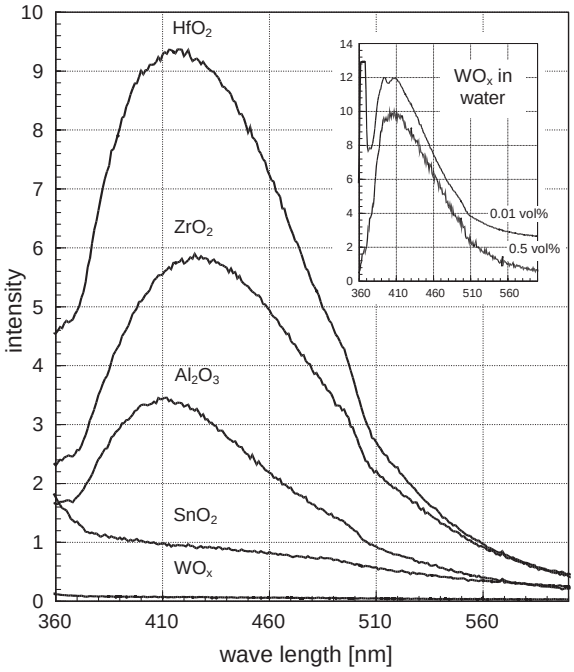


*Figure 4.* Luminescence of different ceramic nanoparticles as powder coated with m-PMMA. The insert shows the luminescence spectra of $WO_x$ suspended in water (ca. 0.5 and 0.01 vol%).

this phenomenon is $WO_x$/m-PMMA powder showing no luminescence at all. Suspended in water, the luminescence is significant. This is shown in the insert of Figure 4 where the luminescence of two different particle concentrations (ca. 0.5 and 0.01 vol%) in water is shown. The upper line, corresponding to the lower

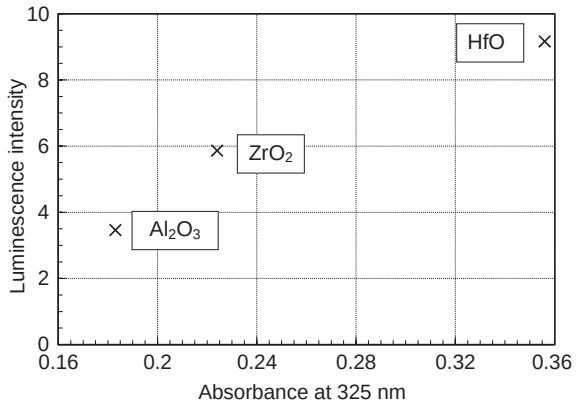


*Figure 5.* Luminescence intensity of the highly insulating oxides $HfO_2$, $ZrO_2$, and $Al_2O_3$ as function of the absorbance at 325 nm of the powders suspended in water with concentrations of 0.01 g $l^{-1}$.

concentration, shows in addition to the luminescence the Raman peak of water at 365 nm, whereas lower curve represents the significantly reduced intensity at higher concentration. In this case, the Raman line of water is completely absorbed. Looking at the highly insulating oxides $HfO_2$, $ZrO_2$, and $Al_2O_3$, one realizes increasing intensity with increasing UV-absorption in the ceramic core. This relationship is demonstrated quantitatively in Figure 5, where the absorbance at 325 nm in aqueous suspension is related to the luminescence intensity.

Besides the dependency on the ceramic core, an additional week dependency on the coating polymer exists. Figure 6 demonstrates this in using alumina as example, showing the luminescence spectra of bare, and polymer-coated alumina kernels. Precursors for polymer coating were MMA, isobutylmethacrylate (IBMA, $H_2C{=}C(CH_3)COOCH_2CH(CH_3)_2$), and 2-isocyanatoethylmethacrylate (IEM, $H_2C{=}C(CH_3)COO(CH_2)_2NCO$); in the case of PTFE, $C_{20}F_{42}$ was selected. As the size of the alumina kernels is in the range from 5 to 8 nm it is known that they are not crystallized (Vollath, 1993). Except for the weak effect caused by PTFE, coated alumina particles show strong luminescence depending on the type of the polymer. Suspending the nanocomposites in a liquid in high or low concentration leads to identical spectra. Figure 7 shows as comparison the emission spectra of $ZrO_2$/m-PMMA as powder and suspended in water. Except for the Raman peak of water at 365 nm, both of the spectra are essentially identical.

In Figure 8, the excitation and the emission spectrum of $Al_2O_3$/m-PMMA nanocomposites are plotted together. The excitation spectrum was measured at the

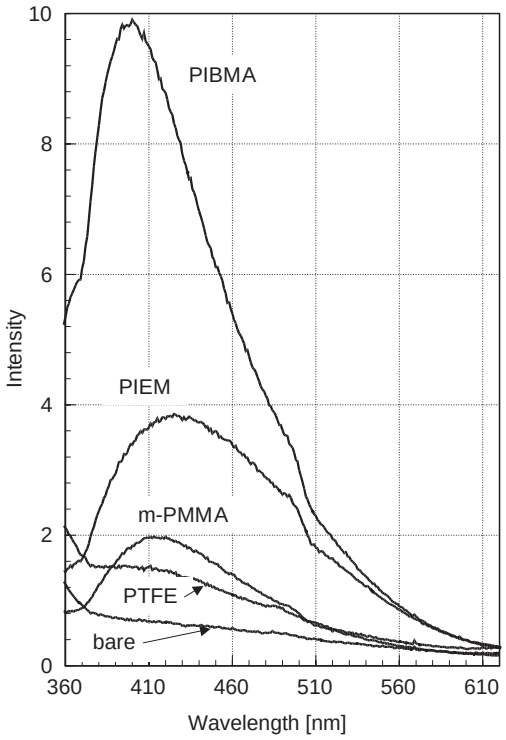


*Figure 6.* Luminescence spectra of $Al_2O_3$ coated with different polymers in comparison to bare alumina showing no luminescence.

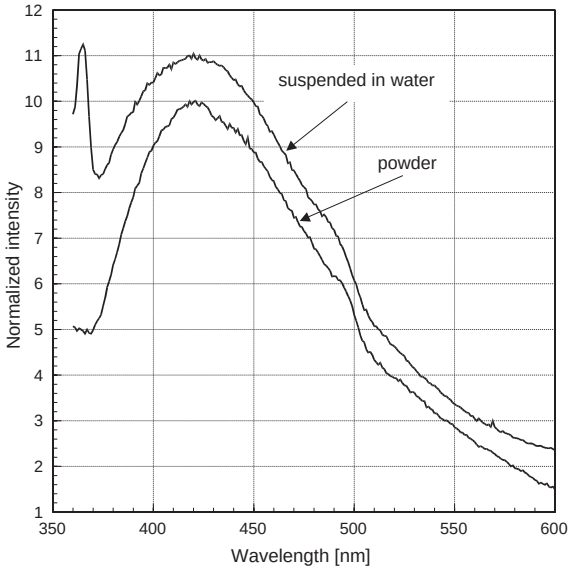


*Figure 7.* Comparison of the luminescence of $ZrO_2$/m-PMMA nanocomposites as powder or suspended in water. The spectra are normalized and stacked. The peak at 365 nm is the Raman line of water.

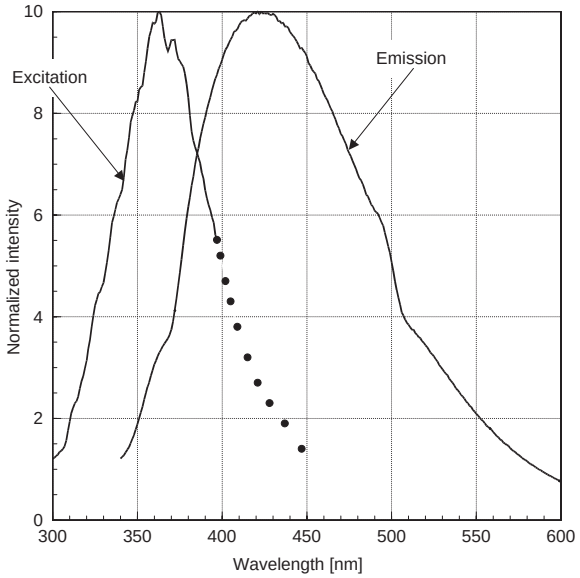


*Figure 8*. Excitation and emission spectra of $Al_2O_3$/m-PMMA nanocomposite particles. For the nanocomposites, the excitation was determined for the maximum at 529 nm. The dotted line is the estimated continuation of the excitation spectrum.

intensity maximum of the emission at 425 nm. Like the emission spectrum, the excitation spectrum shows a broad feature with a maximum at 362 nm. The relationship shown in Figure 8 for the $Al_2O_3$/m-PMMA composite is not altered significantly by exchanging the ceramic core. This result could be expected by the similarity of the emission spectra displayed in Figure 4 for ceramic/polymer composites using different ceramic cores.

To check the influence of the particle size, a series of $ZrO_2$/m-PMMA nanocomposites with different size of the ceramic core were synthesized. Figure 9 shows the results of the measurements of the luminescence. From this graph, it is obvious that the luminescence intensity decreases with increasing particle size. Additionally, a remarkable blue shift with decreasing particle diameter is observed. The particle size was estimated with a precision of ca. $\pm 0.2$ nm by evaluation of X-ray diffraction lines using the Scherrer Formula (Scherrer, 1918). Intensity, position of the emission maximum, and the width of the emission line as function of the particle size are summarized in Table 1.

The appearance of the luminescence spectra is entirely different in the case that the oxide nanoparticles itself depicts luminescence. As example of this group, the composite ZnO/m-PMMA is selected. Figure 10a displays the luminescence spectra of a dry powder

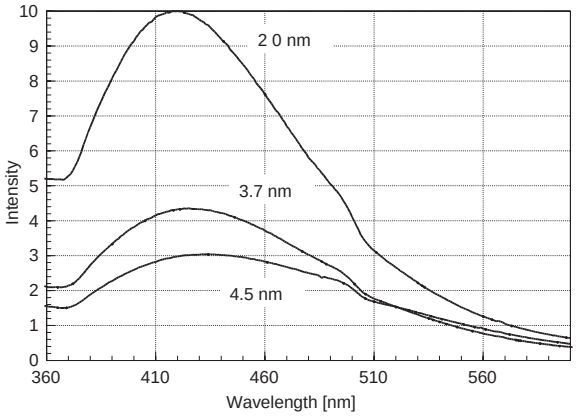


*Figure 9*. Influence of the particle size of $ZrO_2$/m-PMMA nanocomposites on the emission spectra. Exact numbers for the intensity and position of the emission maxima are given in Table 1.

*Table 1*. $ZrO_2$/m-PMMA nanocomposites: wavelength, width, and intensity of the emission of the luminescence as function of the particle diameter

| Particle diameter (nm) | Wavelength of the emission maximum (nm) | Width of the emission line ($nm^{-1}$) | Intensity of the emission maximum (a.u.) |
|---|---|---|---|
| 2.0 | 418 | $4.13 \times 10^{-4}$ | 8.36 |
| 3.7 | 426 | $5.20 \times 10^{-4}$ | 3.64 |
| 4.5 | 434 | $5.40 \times 10^{-4}$ | 2.54 |

with a particle size of ca. 5 nm and the same powder suspended in water with a concentration of $1.2\,g\,l^{-1}$. In this graph, one realizes the excitation lines in first (325 nm) and second (650 nm) order and for both spectra a broad emission band consisting of two maxima at 496 and 529 nm. The luminescence spectrum of the powder suspended in water additionally shows a relatively sharp emission line at 370 nm. The Raman line, appearing at 365 nm, is absorbed by the high concentration of nanoparticles in the suspension. Figure 10b depicts the influence of the particle size on the emission spectrum of ZnO/m-PMMA nanoparticles as powder. These spectra are normalized and stacked. The particle size was determined by electron microscopy, as the determination by X-ray diffraction line profile analysis leads, because of overlapping diffraction lines, to unreliable results. Therefore, the precision of the size determination is poorer and is estimated to be ca. $\pm 0.3$ nm.

Table 2 gives the values of the position of the first and the second intensity maximum as a function of the particle size together with the intensity ratio

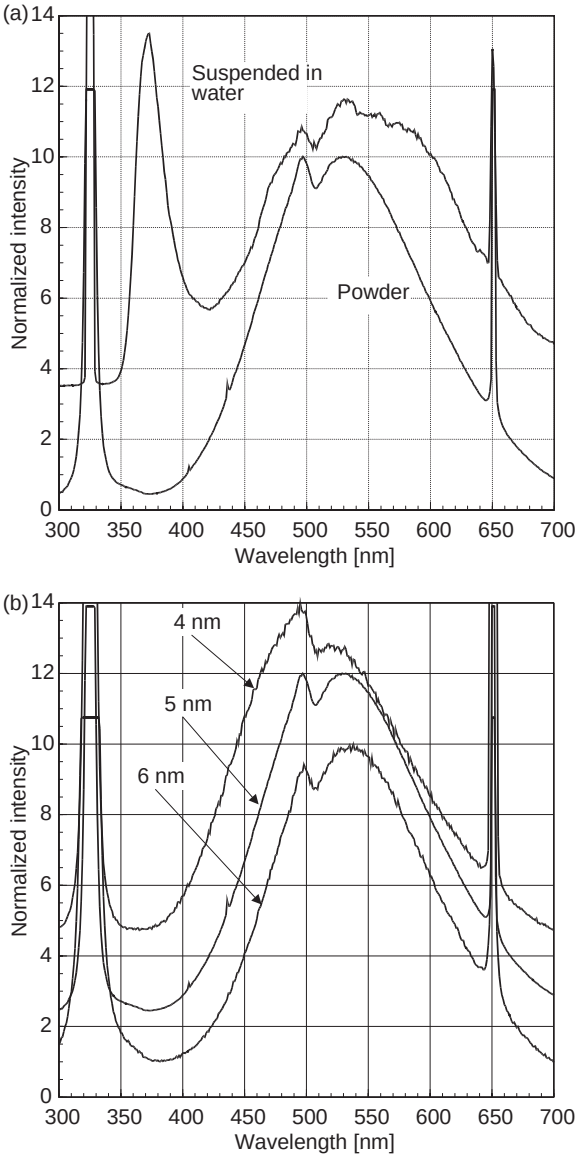


*Figure 10*. Emission spectra of ZnO/m-PMMA nanocomposites. Additionally, the spectra show the exciting line in first order at 325 and at 650 nm in second order. (a) Emission spectra of ZnO/m-PMMA nanocomposites as powder and suspended in water with 1.2 g $l^{-1}$. The size of the ZnO kernels was ca. 5 nm. (b) Influence of the particle size on the luminescence emission of ZnO/m-PMMA nanocomposites.

of these two peaks. One realises a strong blue shift with decreasing particle size of the second and a less pronounced one of the first maximum. Additionally, the intensity ratio of the second over the first peak increases with increasing particle size.

*Table 2*. Influence of the particle size on the wavelength and intensity of the emission spectrum of ZnO/m-PMMA nanocomposites

| Particle size (nm) | Position of the first maximum (nm) | Position of the second maximum (nm) | Intensity ratio of the second over the first maximum |
|---|---|---|---|
| 4 | 495 | 519 | 0.89 |
| 5 | 497 | 530 | 1.0 |
| 6 | 498 | 535 | 1.06 |

## Discussion

It was demonstrated that many oxide nanoparticles show luminescence, provided they are coated with a polymer. IR-absorption studies have revealed the nature of the bonding between the oxide cores and the coating. Based on these results, depicted in Figure 2, it is obvious that during the PMMA coating process a substantial number of ester groups is transformed into the corresponding carboxylates and are chemisorbed at the surface of the oxide with an ester-like linkage (Meyer et al., 1994; Weng et al., 2003). This bonding to the oxide surface lastly explains the lack of solubility in THF. Similar observations of chemisorbed PMMA at the surface of conventional $Al_2O_3$ were reported earlier (Konstadinidis et al., 1992; Papirer et al., 1994). Therefore, more precisely, the oxide ceramic particles are coated with a m-PMMA, independently of the precursor MAA or MMA. Additionally, the precursor molecules of the monomer are polymerized under the influence of the UV-radiation of the microwave plasma and temperature. Therefore, except for a few percent of the polymer precursor not bound to the particle, that are soluble in THF, one may describe a composite particle consisting of a ceramic core and a polymer coating as one molecule.

At first, the source of luminescence of the coated nanoparticles is sought. Experimental results presented in this paper suggest that the luminescence spectra are nearly independent of the oxide core and, except for PTFE, the polymer used for coating. This leads to a first assumption that these spectra are related to the Raman Effect. It was demonstrated earlier (Vollath et al., 2002) that this assumption could be excluded definitely. Looking at the luminescence spectra of the insulating oxides $Al_2O_3$, $ZrO_2$, and $HfO_2$, one realises increasing luminescence intensity with increasing UV-interaction. This is plotted in Figure 5, depicting the luminescence intensity of these wide band insulators as a function

of the UV-absorbance at 325 nm. This graph clearly demonstrates a strong correlation between these two variables, indicating that the primary process of photon absorption occurs – with high probability – in the ceramic core.

As these spectra can be attributed neither to the ceramic core nor to the polymer coating one may rather assume that this luminescence is a phenomenon originating from the interface oxide/polymer. To prove this assumption, the luminescence intensity of $ZrO_2$/m-PMMA nanoparticles was determined as a function of the particle size. From the results plotted in Figure 8 two conclusions can be drawn: (i) The luminescence intensity increases with decreasing particle diameter and (ii) the emission maximum undergoes a blue shift with decreasing particle diameter. Detailed data for these findings are given in Table 1 and plotted in Figure 11a and b. For the dependency of the luminescence intensity as function of the particle size one finds the relation:

$$I = I_0 + \frac{b}{d} \tag{1a}$$

($I$ is intensity, $I_0 = -2.04 \pm 0.1$, $b = 20.8 \pm 0.1$ nm are constants, and $d$ is particle diameter in nanometer). In the size range of particles, were Formula (1a) was fitted; the luminescence intensity is directly proportional to the surface of the particles. This is, because for a given quantity of material, the number of particles is proportional $d^{-3}$, whereas the surface of one particle is proportional $d^2$. Therefore, the surface of a given quantity of particulate matter is proportional $d^{-1}$. The direct proportionality between intensity of luminescence and particle surface promotes the idea that the interface ceramic/polymer is the source of the luminescence. Additionally, a description of the intensity relation of the type

$$I = I_0 \exp(-bd) \tag{1b}$$

($I$ is luminescence intensity, $I_0 = 21.9 \pm 0.4$ and $b = 0.482 \pm 0.007$ nm, and $d$ is particle diameter in nanometer) was analysed. Both Formulae (1a) and (b) describe the experimental values equally well.

The relationship expressed by Formula (1a) clearly suggests that the emission is related to the interface ceramic/polymer of the particles. This finding combined with the correlation drawn from Figure 5, together, are a strong indicator for an excitation process starting with absorption in the oxide particle core, followed by a transfer to the interface, where the emission occurs. Additionally, both descriptions lead to

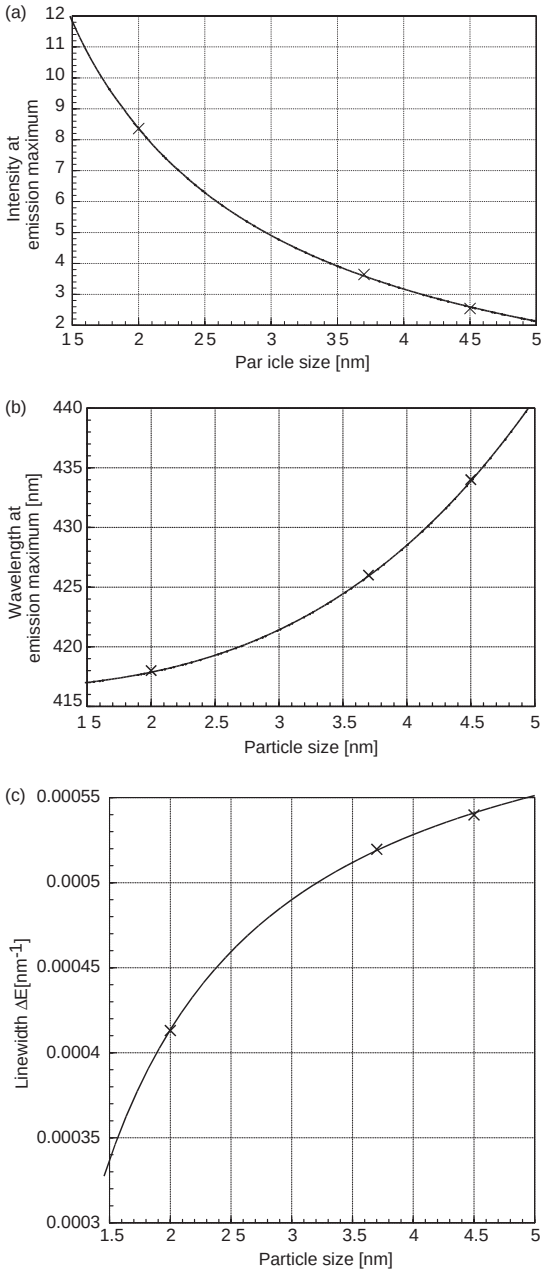


*Figure 11.* Influence of the particle size on the luminescence of $ZrO_2$/m-PMMA nanocomposite powders. (a) Dependency of the luminescence intensity as a function of the particle size measured at the maximum. The experimental data are fitted with a function of the type $I = I_0 + b/d$. (b) Wavelength of the emission maximum as a function of the particle size determined at the maximum of the intensity. The experimentally found blue shift with decreasing particle size is fitted by $\Delta(1/\lambda) = bd^3$. (c) Width of the emission line at half intensity of the maximum. The experimental data are fitted using the function $\Delta E = \Delta E_0 - b/d$.

diminishing small luminescence intensities for particle sizes larger than ca. 10 nm. Probably, this is the reason why this phenomenon was not found earlier.

From the data depicted in Table 1 and Figure 11b, it is obvious that the wavelength of the emission maximum is strongly dependent on the particle size. The wavelength of the emission maximum as function of the particle size follows the relationship:

$$\frac{1}{\lambda} = \frac{1}{\lambda_0} + bd^3 \quad \text{or} \quad \Delta\left(\frac{1}{\lambda}\right) = bd^3 \tag{2}$$

The fitted parameters are $\lambda_0 = 416.5 \pm 0.05\,\text{nm}$, $b = -1.061 \times 10^{-6} \pm 5 \times 10^{-9}\,\text{nm}^{-4}$. In literature, a size dependent blue shift is, in most cases, taken as indication for quantum confinement phenomena. Formula (2) describes a mechanism, expressed by the mathematical description, fundamentally different from quantum confinement in semi-conductor quantum dots. Theoretically, for quantum dots the exponent $n$ in Formula (2) is expected to be $-2$ (Brus, 1984) or $-3$ (Monticone et al., 1998). For quantum confinement systems, published experimental values for the exponent $n$ are strongly scattering in the range from $-1.16$ to $-6$ (Micic et al., 1996; Fu & Zunger, 1997; Albe et al., 1998; Sun et al., 2001). Glinka et al. (2001) found a different mechanism for the blue shift in silica with decreasing particle size based on self-trapped excitons following also an exponential law with negative exponent close to 2. All the mechanisms of blue shift published until now show in contrast to the one observed with oxide/polymer nanocomposites a negative exponent. The blue shift of the luminescence emission of oxide/m-PMMA nanocomposites exhibits the positive exponent 3.

Similarly, to the blue shift with decreasing particle size, a reduction of the line width at half-maximum intensity with decreasing particle size was observed. The reduction of the line width follows the relation:

$$\Delta E = \Delta\left(\frac{1}{\lambda}\right) = \Delta E_0 + \frac{b}{d} \tag{3a}$$

($\Delta E_0 = 6.43 \times 10^{-4} \pm 2.2 \times 10^{-6}\,\text{nm}^{-1}$, $b = -4.59 \times 10^{-4} \pm 6.3 \times 10^{-6}$).

The experimental data, together with the fitting, are plotted in Figure 11c. A fit of equal precision is obtained using the function:

$$\Delta E = \Delta\left(\frac{1}{\lambda}\right) = \Delta E_0 \times (1 - \exp(-bd)) \tag{3b}$$

($\Delta E_0 = 5.73 \times 10^{-4} \pm 1.6 \times 10^{-6}\,\text{nm}^{-1}$, $b = 6.39 \times 10^{-1} \pm 5.8 \times 10^{-3}\,\text{nm}$.

Formulae (3a) and (b) express a reduction of the line width with decreasing particle size. The blue shift together with the reduction of line width indicate that the emission is directly related to the size of the nanoparticle, because the gap to the conduction band is increasing and the width of the bands are decreasing with decreasing particle size. Insofar, both findings are equivalent describing a strong correlation of the emission with the band structure of the oxide core.

From biacetyl, $CH_3$–(C=O)–(C=O)–$CH_3$, it is well known that the carbonyl group is responsible for luminescence in aliphatic compounds (Parker, 1968). Therefore, one may assume that in the m-PMMA system, where a carbonyl group is close to the ceramic surface a similar mechanism is acting. To prove this assumption, the smallest molecule having a carboxylate group that may bind similarly to the ceramic surface, formicacidethylester, H–(C=O)–O–$CH_3$ (FAME), was selected to coat the oxide particles instead of MMA. It is expected that these molecules are, similarly as m-PMMA, bond to surface forming H–(C=O)–O– (oxide particle). If this assumption is correct, spectra similar to the ones obtained after coating with m-PMMA are expected. To get unequivocal conditions at the outside, the particles were coated additionally with PHPMA. Oxide particles coated with PHPMA show only very weak luminescence because with a high probability the $(OH)^-$ group binds to the surface. This experiment was performed with $ZrO_2$ as ceramic core. The luminescence spectrum of these particles is shown in Figure 12. For the powder, the emission spectrum is nearly identical to the one found with m-PMMA coated materials as it is shown in Figures 4 and 6. This is insofar remarkable as aqueous solutions of formicacidmethylester show luminescence with a few isolated lines in the UV. These findings indicate that there is a high probability that the carbonyl group of these compounds is responsible for the emission spectrum. To remove last doubts, the surface was covered with a compound without carbonyl group. For this experiment diethylether (DEE), $C_2H_5$–O–$C_2H_5$, was selected. It is assumed that this leads to particles of the type $C_2H_5$–O–($ZrO_2$). Similar as in the case of FAME, the outside of the particles was coated with PHPMA. The luminescence spectrum of this composite is plotted in Figure 12, too. Additionally, for information, the spectrum of $ZrO_2$/PHPMA composites is also given. For the material coated with DEE, one realizes an entirely different spectrum as compared to the ones related to compounds with a carbonyl group directly adjacent

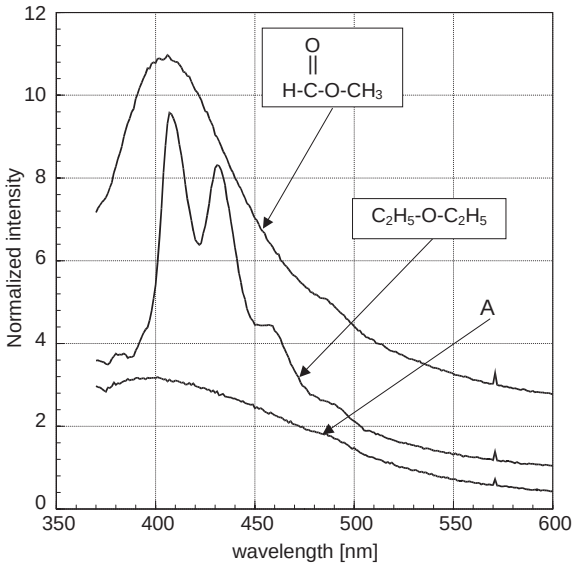


*Figure 12.* Luminescence spectrum of nanocomposite powders with $ZrO_2$ kernels coated with FAME and DEE. The outside of the composites is coated with PHPMA. Additionally, the weak emission spectrum of $ZrO_2$ coated with PHPMA (A) is given for comparison. The spectra are normalized and stacked.

to the surface. Combining this result with the finding, that luminescence of oxide/m-PMMA nanocomposites is a surface related phenomenon indicates clearly that the carbonyl group directly adjacent to the surface is responsible for luminescence in these systems.

Finally, one can look into the emission spectra of zinc oxide. Zinc oxide is a semi-conducting oxide well known for its strong luminescence in the UV and green region. In this study, the ZnO/m-PMMA nanocomposite powders show a split peak in the range between 450 and 550 nm. Additionally, as demonstrated in Figure 10a, in aqueous suspensions the UV-peak at 370 nm is visible, too. Looking at the peaks in the visible range, one may assume that one of these peaks is connected to the interaction of the polymer with the ceramic core. In literature, for ZnO powder one usually finds the broad emission in the visible range, whereas the UV-emission around 370 nm is typically found in organic capped ZnO particles (Guo et al., 2000). These authors show that the intensity of the UV-peak depends strongly on the amount of polyvinylpyrrolidone (PVP) in a ZnO/PVP mixture. The intensity increased with increasing PVP content in the mixture. It is of special importance that the UV-peak was not found in the case of pure pressed and sintered ZnO. This is compatible with our finding that the UV-peak was found only in aqueous suspensions. In contrast, Mitra and Thareja (1999) found this UV-emission at a wavelength of 395 nm in pressed and sintered pure ZnO powder with grain size significantly larger than 20 nm, after pumping with more than 5 $MWcm^{-2}$.

The broad emission in the visible range, in this study observed with two maxima at 496 and 529 nm, is generally observed unsplit in other studies. Depending on the environment and particle size, the maximum is at 500 nm (Monticone et al., 1998), 520 nm (Guo et al., 2000), or 605 nm (Cao et al., 2000). A similar splitting of the emission in the visible range was found by Fujihara et al. (2001) on ZnO particles with a size of 6.2 nm embedded in $MgF_2$ films. This result, together with the ones presented in Figure 10a suggests that the splitting is a consequence of the interaction of the ZnO particles with the surrounding material. Therefore, the first maximum at 496 nm, found in this study, is attributed to the surface interaction with the polymer and the maximum at 529 nm to the ZnO emission. The peak, attributed to the interaction with the polymer, shows, similar as in the case of insulating oxides, a blue shift with decreasing particle size (Table 2). Compared to the insulating oxides, for ZnO this maximum is shifted ca. 100 nm to the red. The reason for this difference is not clear yet.

To shed more light into the luminescence behaviour of ZnO/m-PMMA nanocomposites, the influence of the particle size was analysed in detail. Figure 13a shows the wavelength of the emission maximum as function of the particle size. The experimental data are fitted with:

$$\frac{1}{\lambda} = \frac{1}{\lambda_0} + bd^{-3} \quad \text{or} \quad \Delta\left(\frac{1}{\lambda}\right) = bd^{-3} \tag{4}$$

($\lambda_0 = 542.7 \pm 0.4$ nm, $b = 5.61 \times 10^{-3} \pm 1 \times 10^{-4}$ $nm^{-2}$). The exponent $-3$ is the same as it was found by Monticone et al. (1998) for the blue shift in ZnO related to quantum confinement. As shown in Figure 13a, besides of the relatively poor determination of the particle size, this fit is nearly perfect.

Because of the small variation, analysing the blue shift of the first emission peak around 487 nm makes no sense. Instead of the wavelength, the intensity ratio of the second over the first peak is evaluated. The following relation describes this ratio as function of the particle size:

$$\frac{I_2}{I_1} = A + kd^{-2} \tag{5}$$

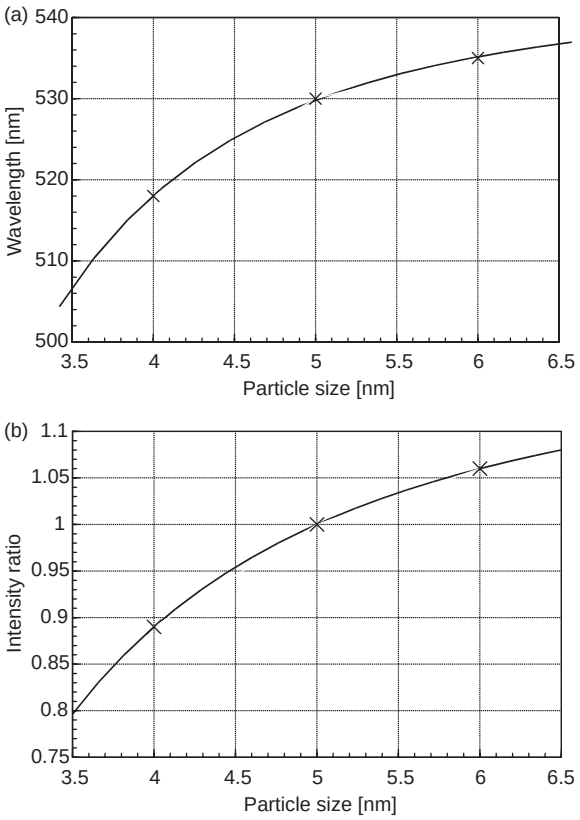


*Figure 13.* Influence of the particle size on the emission spectra of ZnO. (a) Blue shift of the ZnO emission line with decreasing particle size. The experimental points were fitted with $1/\lambda = 1/\lambda_0 + bd^{-3}$. (b) Intensity ratio of the quantum confinement peak over the oxide–polymer interaction peak. The experimental points follow the function $I_2/I_1 = A + kd^{-2}$.

($I_2$, $I_1$ are intensity of the second or first peak, respectively, $A = 1.120 \pm 2 \times 10^{-4}$ and $k = -4.9 \pm 5 \times 10^{-3}\,\mathrm{nm}^{-2}$). Figure 13b depicts the experimental data together with the fitted function. The exponent $-2$ may be explained easily by the assumption that the intensity of the second peak, caused by quantum confinement, is proportional to the number of particles, $d^{-3}$ whereas the first peak is due to the interaction between the oxide core and the polymer coating, leading, according to Formula (1a) to a proportionality of the intensity with particle size of $d^{-1}$. Therefore, this ratio follows a proportionality with $d^{-3}/d^{-1} = d^{-2}$, clearly indicating that the first peak in the emission spectrum is related to the oxide/polymer interaction.

## Conclusions

Besides the well-known semi-conducting oxides, nanoparticles consisting of an insulating oxide ceramic exhibit luminescence provided they are coated with a polymer. Nanocomposites of this type are synthesised using the Karlsruhe Microwave Plasma Process. Even when it was not possible to clarify the mechanism of luminescence in ceramic/polymer nanocomposites in detail, experimental results suggest a relation of the luminescence to the interface kernel/coating. The exciting UV-quanta are absorbed in the ceramic core and the excitation is transferred from the ceramic core to the interface kernel/coating, where the emission occurs. As the luminescence of these oxide/polymer nanocomposites is proportional to the surface, it is possible to tailor wavelength and intensity of the luminescence by changing the particle size. Certainly, also the oxide of the core is a handle to tune the emission. In the case of semi-conducting oxides, such as ZnO, a mixture of the quantum confinement mechanism with the surface interaction mechanism is observed.

Looking at the large overlapping between the excitation and emission spectra of the nanocomposites discussed in this paper, one realises that these coated particles are ideally suited for nanophotonic waveguides for the transport of electromagnetic energy using the Förster mechanism (Förster, 1948a,b). Lastly, it is important to mention that the oxide/m-PMMA nanoparticles are neither toxic nor carcinogenic simplifying the handling and application of luminescent nanoparticles.

## References

Albe V., C. Jouanin & D. Bertho, 1998. Phys. Rev. B 58, 4713.
Brus L.E., 1994. J. Chem. Phys. 80, 4403.
Cao H., J.Y. Xu, S.-H. Chang & S.T. Ho, 2000. Phys. Rev. E, 61, 1985.
Chen Y., Y. Cao, Y. Bai, W. Yang, J. Yang, H. Jin & T. Li, 1997. J. Vac. Sci. Technol. B 15, 1442.
Faguy P.W., W.R. Fawcett, G.J. Liu & A.J. Motheo, 1992. J. Electr. Chem. 339.
Förster V.T., 1948a. Ann. Phys. 6, 54–75.
Förster V.T., 1948b. Naturwissenschaften 33, 93–100.
Fu H. & A. Zunger, 1997. Phys. Rev. B 55, 1642.
Fujihara S., H. Naito & T. Kimura, 2001. Thin Solid Films 389, 227–232.

Glinka Y.D., S.-H. Lin, L.-P. Hwang, Y.-T. Chen & N.H. Tolk, 2001. Phys. Rev. B 64, 085421.
Guo L., S. Yang, C. Yang, P. Yu, J. Wang, W. Ge & G.K.L. Wong, 2000. Chem. Mater. 12, 2268–2274.
Konstadinidis K., B. Thakkar, A. Chakraborty, L.W. Potts, R. Tannenbaum, M. Tirrell & J.F. Evans, 1992. Langmuir 8, 1307.
Lamparth I., D.V. Szabó & D. Vollath, 2002. Macromol. Symp. 181, 107.
Meyer T.J., G.J. Meyer, B.W. Pfennig, J.R. Schoonover, C.J. Timpson, J.F. Wall, C. Kobusch, X. Chen, B.M. Peek, C.G. Wall, W. Ou, B.W. Erickson & C.A. Bignozzi, 1994. Inorg. Chem. 33, 3952.
Micic O.I., J. Sprague, Z. Lu & J. Nozik A., 1996. Appl. Phys. Lett. 73, 3150.
Mitra A. & R.K. Thareja, 1999. Mod. Phys. Lett. B 13, 1075–1080.
Monticone S., R. Tufeu & A.V. Kanaev, 1998. J. Phys. Chem. B 102, 2854–2862.
Pandya N., D.W. Muenow, S.K. Sharma & B.L. Sherriff, 1994. J. Non-Cryst. Solids 176, 140–146.
Papirer E., J.-M. Perrin, G. Nanse & P. Fioux, 1994. Eur. Polym. J. 30, 985–991.
Parker C.A., 1968. Photoluminescence of Solutions. Elsevier, Amsterdam, p. 21.
Porteanu H.E., E. Lifshitz, M. Pflughoefft, A. Eychmüller & H. Weller, 2001. Phys. Stat. Sol. B 226(1), 219.
Roth P., 2000. Private Communication.
Scherrer P., 1918. Göttinger Nachrichten, Math. Phys. 98–100.
Socrates G., 1994. Infrared Characteristic Group Frequencies. John Wiley & Sons, Chichester.
Sun C.Q., T.P. Chen, B.K. Tay, S. Li, H. Huang, Y.B. Zhang, L.K. Pan, S.P. Lau & X.W. Sun, 2001. J. Phys. D 34, 3470–3479.
Tian Y., T. Newton, N.A. Kotov, D.M. Guldi & J.H. Fendler, 1996. J. Phys. Chem. 100(21), 8927.
Vollath D., 1993. KfK Nachrichten 25, 139.
Vollath D., 1994. German Patent G9403581.4.
Vollath D. & D.V. Szabó, 1994. Nanostruct. Mater. 4, 927.
Vollath D., D.V. Szabó & B. Seith, 1998. German Patent DE19638601C1.
Vollath D., D.V. Szabó & J. Fuchs, 1999. Mat. Res. Soc. Symp. Proc. 577, 443.
Vollath D., 2001. German patent application, DE 101 54988.1.
Vollath D., I. Lamparth & D.V. Szabó, 2002. Mat. Res. Soc. Symp. Proc. 703, V7.8.1
Wang Y., H. Cheng, L. Zhang, Y. Hao, J. Ma, B. Xu & W. Li, 2000. J. Mol. Catal. A 151, 205.
Weng Y.-X., L. Li, Y. Liu, L. Wang & G.-Z. Yang, 2003. J. Phys. Chem. B 107, 4356.